Open access • Journal Article • DOI:10.1002/ADMA.201805367

Carbon-Based Metal-Free Catalysts for Electrocatalytic Reduction of Nitrogen for Synthesis of Ammonia at Ambient Conditions. — Source link

Shenlong Zhao, Xunyu Lu, Lianzhou Wang, Julian D. Gale ...+1 more authors

Institutions: University of New South Wales, University of Queensland, Curtin University

Published on: 01 Mar 2019 - Advanced Materials (Adv Mater)

DOI: 10.1002/adma.201805367

Article type: Research News

Carbon-Based Metal-Free Catalysts for Electrocatalytic Reduction of Nitrogen for Synthesis of Ammonia at Ambient Conditions

*Shenlong Zhao, Xunyu Lu, Lianzhou Wang, Julian Gale, and Rose Amal**

Keywords: metal-free catalysts, nitrogen-doped carbons, electrocatalysis, nitrogen reduction reaction

Abstract

The electrocatalytic nitrogen reduction reaction (NRR) is a promising catalytic system for N_2 fixation in ambient conditions. Currently, metal-based catalysts are the most widely studied catalysts for electrocatalytic NRR. Unfortunately, the low selectivity and poor resistance to acids and bases, the low Faradaic efficiency, production rate, and stability of metal-based catalysts for NRR make them uncompetitive for the synthesis of ammonia in comparison to the industrial Haber-Bosch process. Inspired by applications of carbon-based metal-free catalysts (CMFCs) for oxygen reduction reaction (ORR) and CO_2 reduction reaction (CO_2RR), the studies of these CMFCs in electrocatalytic NRR have attracted great attention in the past year. However, due to the differences in electrocatalytic NRR, there are several critical issues that need to be addressed in order to achieve rational design of advanced carbon-based metal-free electrocatalysts to improve activity, selectivity, and stability for NRR. This research news presents the recent developments in the field of carbon-based metal-free NRR catalysts,

along with critical issues, challenges, and perspectives concerning metal-free catalysts for electrocatalytic reduction of nitrogen for synthesis of ammonia at ambient conditions.

1. Introduction

Ammonia (NH_3), a key precursor for fertilizer production, convenient hydrogen carrier, and emerging clean fuel, is one of the most essential industrial chemicals for both human beings and earth's ecosystem.[1] Presently, the worldwide production of ammonia is more than 145 million metric tons annually that is mainly produced by the industrial Haber-Bosch process.[2] In the Haber-Bosch process, the reaction of a mixture of hydrogen gas (H_2) and nitrogen gas (N_2), termed synthesis gas, is catalyzed by an iron-based catalyst at high temperature and pressure to overcome the thermodynamic barrier related to the dissociative mechanism.[3] Moreover, recycling of unreacted synthesis gas is required due to the limited conversion (~ 15%) of each pass. Though a high overall conversion (~ 97%) can be achieved by the utilization of these unreacted gases, it accounts for 1% to 3% of the world's annual energy production, making it a significant contributor to energy and environmental challenges.[4] In addition, the large plant infrastructure required is generally only economically viable at large economies of scale, where natural gas feedstock is responsible for 50% of the production cost.[4c] Therefore, it is highly desirable to develop an alternative sustainable approach for ammonia synthesis. To this end, the electrocatalytic nitrogen reduction reaction (NRR), producing ammonia from water and atmospheric nitrogen at room temperature, is a rapidly growing field of research.

Since the electrocatalytic NRR was discovered by Davy et al. in 1807,[5] metal-based materials (e.g. Au, Pt, Ru, Mo, Ni, Fe_2O_3) have been the most widely used catalysts.[6] Among them, transition metal-based catalysts are generally considered as promising catalysts to relieve the kinetic issues for

activation of the stronger N≡N bond due to the availability of d-orbital electrons for the π-back donation process.[7] In the past few years, many efforts have been made to improve the performance of transition metal-based NRR electrocatalysts.[3, 8] Unfortunately, the ammonia yield and Faradaic efficiency of these reported metal-based electrocatalysts are much lower compared to the demand of practical applications, which mainly originates from the following points: First, the adsorption of N_2 molecules on metals is poor due to unfavorable contact on the metal-based catalyst surfaces, thereby seriously impeding the yield of NRR.[8b] Second, the bond strength between nitrogen and metal is too weak for N_2 activation and the d-orbital electrons in transition metals favor the formation of metal-H bonds leading to the adverse hydrogen evolution reaction (HER),[9] both of which compromise the Faradaic efficiency. Besides, the intrinsic structural features, such as low surface area and porosity, are unfavorable for nitrogen fixation, making it an obstacle for industrial-scale application.[10] Therefore, exploitation of new classes of electrocatalysts is necessary to achieve transformative advances in the electrochemical N_2 fixation field.

Carbon-based metal-free catalysts (CMFCs) are a new class of alternatives to metal-based catalysts.[11] In the past ten years, various CMFCs, including heteroatom-doped carbon dots, carbon nanotubes, graphene, and graphite, have attracted worldwide attention as efficient metal-free catalysts for advanced energy conversion including oxygen reactions,[12] hydrogen evolution reaction,[13] CO_2 reduction reaction (CO_2RR)[14] and bi/multi-functional catalysis.[15] Certain carbon-based metal-free materials have been demonstrated to be stable and effective metal-free electrodes for Zn-air batteries and self-powered water-splitting systems.[15b, 16] Indeed, carbon-based metal-free materials, formed by strong covalent bonding between carbon atoms, are also ideal candidates for designing high-performance NRR electrocatalysts owing to their numerous unique physical and

chemical properties including high surface area, excellent conductivity, controllable porosity, and abundant defects.[17] For example, the hierarchical pore structure and excellent conductivity of carbon materials are the basic preconditions for the accessibility between reactants (N_2) and active sites, mass transfer and electron transfer.[18] Moreover, heteroatoms doping such as B, N and P could effectively tune the energy bandgap, spin density and charge density, regulating the competition between NRR and HER through synergistic electron transfer interactions between the dopants and surrounding carbon atoms.[19] Last but not least, carbon-based metal-free materials are generally made up of earth-abundant elements such as C, B, N and O, which makes them superior in terms of cost to noble metal or metal-based materials for practical applications.[20]

Here, we summarize the state-of-the-art research activities in CMFCs for electrochemical NRR under ambient conditions. We present the progress in the application of heteroatom-doped CMFCs in NRR. After that, the fabrication and application of structure/defects-controlled CMFCs for electrochemical nitrogen fixation are discussed. Finally, the challenges and future opportunities in this exciting field are also presented.

2. Heteroatom-doped carbon-based metal-free NRR catalysts

2.1. Nitrogen doping

The origin of the activity of metal-free catalysts has been attributed to the strong electronic affinity of heteroatoms and substantially high positive charge density on the adjacent carbon atoms.[21] It was revealed by using quantum mechanical calculations based on hybrid density functional theory (DFT) that the doping-induced charge redistribution could greatly enhance the chemisorption of reactants such as O_2 and CO_2 with a lower overpotential.[11, 22] Recent studies have

shown that the effect of nitrogen doping could be extended to electrocatalytic NRR.[1d, 23] N-doped porous carbons (NPC) were synthesized by pyrolyzing the zeolite imidazolate framework (ZIF) at 750, 850, or 950 °C (denoted as NPC-750, NPC-850, and NPC-950) for electrocatalytic NRR under ambient conditions (**Figure 1**A, B).[23] The carbon materials obtained not only preserve the features of ZIF precursors, including high surface area and abundant pores, but pyrolysis also induces the formation of defects and charge polarization, providing a great number of active sites and fast mass transfer for N_2 adsorption and N≡N splitting.[24] N_2 adsorption-desorption isotherms (**Figure 1**C) have shown that NPC-750 possesses a high surface area of 896 cm^3 g^{-1}, while the intensity ratios of D and G bands (I_D/I_G) in Raman spectra were as high as 1.04, suggesting that many defects or sp^3-C bonds were created. Subsequently, the NPC catalysts were used for nitrogen fixation by electrolyzing N_2 at constant potential. It should be noted that the NRR performance of NPCs was evaluated in 0.05 M H_2SO_4 by employing Nessler's reagent spectrophotometry. **Figure 1**D shows the ammonia production rate increases with increasing the applied overpotential in N_2 saturated solution, while there is no detectable ammonia in Ar saturated solution, demonstrating that ammonia is generated from the dissolved N_2 rather than the nitrogen atoms of NPC. Moreover, the optimized ammonia production rate of NPC-750 (0.84 μmol cm^{-2} h^{-1}) is one order of magnitude higher than those of reported metal-based NRR catalysts including Ru,[25] Au[26] and Fe/CNT[27] (0.012-0.097 μmol cm^{-2} h^{-1}). Besides the ammonia production rate, the Faradaic efficiency (FE) of NPC-750 is also investigated. As shown in **Figure 1**D, a maximum FE of 1.42% is obtained for ammonia fixation on NPC-750, higher than those from the recently reported electrocatalysts under similar conditions.[6a, 28]

To understand the catalytic mechanism of NPC for NRR, a suite of experiments and computational calculations were carried out. N_2-temperature programmed desorption (TPD) curves

and double-layer capacitance tests showed that NPC-750 with the highest N content has the largest N_2 desorption peak area and the highest kinetics for electrochemical reduction of N_2 to ammonia. Also, the contribution of N species to NRR was further analyzed by X-ray photoelectron spectroscopy (XPS), indicating that the content of pyridinic N has a strong correlation with the enhancement of NRR activity. The role of different N species toward electrocatalytic NRR was further confirmed by DFT calculations using a N-doped carbon model, where pyridinic, pyrrolic, and graphitic N are considered. Based on the preferable pathway for ammonia synthesis (*N≡N → *NH≡NH → *NH_2-NH → 2NH_3), the Gibbs free energies of the highest intermediates for elementary reaction on pyridinic (0.45 eV) and pyrrolic N (0.56 eV) sites are much lower than those of graphitic N sites (**Figure 1**E, F). From these combined experimental and theoretical results, it can be concluded that the superior NRR activity of NPC-750 should be attributed to its high content of pyridinic and pyrrolic N.

In a similar but independent study, Wu and co-workers reported a series of zeolite imidazolate framework-derived nitrogen-doped nanoporous carbons (C-ZIF-700, C-ZIF-800, C-ZIF-900 and C-ZIF-1100) for electrocatalytic N_2 to ammonia conversion in 0.1 M KOH solution.[1d] Impressively, C-ZIF-1100 exhibits a production rate of NH_3 up to 3.4×10^{-6} mol cm^{-2} h^{-1} with a FE of 10.2 % by using the indophenol test and spectrophotometric analysis to determine the generated NH_3 (**Figure 1**G). On the contrary, the NH_3 production rate of N-doped carbon from polyaniline (PANI) and N-doped carbon tubes derived from dicyandiamide (DCDA) synthesized under identical conditions are much lower relative to that of C-ZIF-1100, highlighting the importance of the framework of the selected precursors. In addition, it is noted that the presence of metals, such as Fe, has a negative effect on ammonia synthesis, since the metals could coordinate with pyridinic N in carbon defects, thereby blocking the potential active sites. Furthermore, the NRR performance of the as-prepared C-ZIF-1100

was also evaluated in acid media (0.1 M HCl). The production rate in 0.1M HCl is nearly one order of magnitude lower than that in 0.1 M KOH at the same test conditions owing to HER being more favorable than NRR in acid media. Apart from the performance studies, possible active sites and reaction pathways of NRR on C-ZIF surface were elucidated through theoretical calculations. The adsorption of N_2 on all the possible N species (pyridinic, pyrrolic, and graphitic nitrogen embedded in a graphene layer) was considered. DFT results indicated that the pyridinic N_3 moiety embedded in a graphitic layer, which contains one protonated pyridinic nitrogen and one adjacent atomic vacancy site, is the unique energetically favorable site for N_2 adsorption (**Figure 1**H). Then, the adsorbed N_2 molecules on the C-ZIF surface are further reduced to form ammonia by a cycling pathway with the carbon matrix. Of particular interest, the predicted N-N bond distance (1.37 Å) of the adsorbed N_2 is larger than that in the N_2 molecule, demonstrating that the N-N triple bond is significantly weakened in this step thus facilitating the cleavage of the strong N-N bond. Predicted free energy evolution of N_2 reduction on N_3 sites in N-doped carbon under electrode potentials of 0 and -0.3 V shows the free energy requirement decreases to 1.45 eV when applying a lower potential, again verifying that the three pyridinic N atoms embedded into carbon planes can adsorb the N_2 molecule for subsequent N≡N bond dissociation.

2.2. Boron Doping

The B-C σ bond is significantly polarized to induce a positive charge on the boron atom owing to the larger electronegativity of carbon (2.55) than that of boron (2.04).[29] Moreover, N_2 is a weak Lewis base, thus, it is ideal to create a Lewis acid catalytic site with an empty orbital to bind N_2 by boron doping.[30] Recently, boron-doped graphene (BG), synthesized by thermal reduction of mixture of H_3BO_3 and graphene oxide, was investigated for electrocatalytic N_2 reduction.[31] Transmission

electron microscopy (TEM) and energy dispersive X-ray spectroscopy (EDS) mapping images (**Figure 2**A, B) revealed the successful substitution of boron into the graphene structure, which was further confirmed by Raman and Fourier transform infrared (FTIR) spectroscopy. The chemical state of the boron dopants in graphene was studied by X-ray photoelectron spectroscopy (XPS). The high-resolution B 1s spectrum of BG (**Figure 2**C) shows three characteristic peaks, corresponding to structures of B_4C (187.8 eV), BC_3 (189.9 eV), BC_2O (191.2 eV), and BCO_2 (192.3 eV).[32] The various boron structures with different electron density distributions may play different roles in its electrocatalytic NRR. The nitrogen adsorption on the BG samples, which is a prerequisite step for NRR, was also examined by temperature-programmed desorption (TPD) (**Figure 2**D). Compared with graphene (G), the chemisorption of N_2 on BG samples was greatly enhanced and exhibited a strong correlation with the boron doping percentage, suggesting that the chemical adsorption sites for N_2 should be attributed to the boron dopants.

Subsequently, the NRR electrocatalytic activities of the samples (BG-1, BOG, BG-2, and G) were evaluated in a N_2-saturated 0.05 M H_2SO_4 solution. As shown in **Figure 2**E, the current increased significantly in N_2-saturated solution compared to that in Ar-saturated media at the same conditions. Especially, there was an enhanced reduction current in the potential interval of -0.45 to -0.70 V vs RHE, implying the reduction of N_2. The amount of ammonia was determined by the reaction of salicylate and nitroprusside into the intense blue indophenol complex. The BG-1 with the highest boron content shows the best catalytic performance, with a NH_3 production rate of 9.8 μg h^{-1} cm^{-2} and an FE (NH_3) of 10.8 % at -0.5 V (**Figure 2**F), which are 5 and 10 times higher than those of the undoped G, respectively. The production rate and FE value obtained from BG-1 are some of the highest values among all the reported NRR electrocatalysts.[6a] To further explore the relationship

between the different boron structures and NRR activity, computational calculations were performed. The distal pathway in the association mechanism ($N_2 \rightarrow N_2^* \rightarrow NNH \rightarrow N^* + NH_{3(g)} \rightarrow NH^* \rightarrow NH_2^* \rightarrow NH_3^* \rightarrow NH_{3(g)}$) was proposed to be the NRR process in this work (**Figure 2**G, H), because it is more likely to stabilize the intermediates than other pathways in the metal-free catalysts.[33] DFT calculations (**Figure 2**H) indicate the free energy (0.43 eV) of the rate-determining step (N* → NH*) for BC_3 is much lower than those of BCO_2 (1.04 eV) and BC_2O (1.30 eV), and the lowest reaction energy barrier for BC_3 explained its superior catalytic NRR activity among these different boron structures.

3. Structure controlled carbon-based metal-free NRR catalysts

In addition to the heteroatom doping, structural control by constructing hierarchical porosity, nano-structuring, and defect engineering is another efficient approach to create/increase the number of active sites.[34] Tunable porous structures also play a key role in enhancing the diffusion of solvated gas molecules such as N_2.[35] Generally speaking, the pore size, pore volume, and interconnected hierarchical pore structure, composed of the combination of macropores, mesopores, or micropores, largely determines the accessibility and enrichment of reactants to active sites (e.g. O_2, CO_2 and N_2) and diffusion dynamics of electrolytes.[36] Recently, the hierarchically structured nitrogen-doped nanoporous carbon membranes (NCMs) were fabricated for electrochemically converting N_2 into NH_3 at room temperature in 0.1 M HCl solution.[18] A high magnification SEM image (**Figure 3**A) reveals that carbon nanotubes (CNTs) are uniformly embedded in the three-dimensionally interconnected microporous NCM, and the BET surface area of the NCM (**Figure 3**B) is 432 $m^2\ g^{-1}$, with a high pore volume of 0.58 $cm^3\ g^{-1}$. The pore size distribution shows the pores traversing the entire micro- to meso- to macro-pore range. Such hierarchically porous

membrane architectures not only provide abundant accessible surface areas, but also offer large mesopores and macropores interconnected in three-dimensional networks that would enhance the three-phase contact and charge transport between the heterogeneous electrocatalyst, aqueous electrolyte, and gaseous reactants. Furthermore, the catalytic properties of the as-prepared NCM for NRR were assessed in acidic media. The yield of NH_3 generated by NRR was examined by using the traditional indophenol blue method. As a result, the maximum FE of 5.2% was obtained at a given potential of -0.2 V and the production rate of NH_3 was up to 0.008 mg cm^{-2} h^{-1} at -0.3 V (**Figure 3**C). Moreover, the selectivity of the NCM electrode to NH_3 is almost 100%. To highlight the significance of the carbon structure, a composite NCM-Au NP electrode was fabricated for NRR. With its unique structure, the NCM-Au NP electrode shows enhanced FE and production rate for NH_3 of 22% and 0.036 mg cm^{-2} h^{-1}, respectively. This finding reveals the key role of electrode structure control in electrochemical nitrogen fixation, and paves the way to designing advanced NRR electrocatalysts.

Defect engineering has also been shown as an alternative way to endow carbon-based metal-free materials with highly active sites. Yu and co-workers demonstrated that the metal-free polymeric carbon nitride (PCN) with abundant nitrogen vacancy (NV) defects are efficient electrocatalysts for nitrogen fixation under ambient conditions.[19] In order to controllably create NVs, the 2D sheet-like PCN prepared by polycondensation of melamine was heated in an Ar atmosphere. The electron paramagnetic resonance (EPR) spectra (**Figure 3**D) were recorded to confirm the introduction of NV by probing unpaired electrons in PCN. As shown in **Figure 3**D, the EPR signal of PCN-NV at a *g value* of 2.0034, assigned to the defects caused by re-distribution of the extra electrons to adjacent carbon atoms through the delocalized π-conjugated networks, is much higher than that of PCN without or with less defects.[37] The presence of the NV defects was further

confirmed by XPS and UV/Vis diffuse reflection spectra. Theoretical calculations were then conducted to show the feasibility of N_2 activation on the PCN with NV defects. Charge density calculations suggested that the electrons on adjacent carbon atoms are favorably transferred to the adsorbed N_2 by the electron back-donation process, which is conducive to activating the N≡N triple bond.[1b, 38] The free energy diagram (**Figure 3**E) reveals the low energy pathways for NRR on NV-engineered PCN. Finally, the NRR performance of PCN with NVs was verified by electrocatalytic testing in acidic media. The superior NRR performance of PCN-NV gave a NH_3 production rate of 8.09 mg h^{-1} $mg^{-1}_{cat.}$ with a FE of 11.59 %, 10 times more than that of the pristine PCN without nitrogen vacancies, highlighting the key role of the NV defects for NRR. Stability of catalysts is another critical factor for practical applications, which can be investigated by cycling and chronoamperometric tests. Cycling tests of catalysts indicates there is no obvious reduction of ammonia yield after 8 cycles (**Figure 3**F). The elemental analysis and EPR spectrum of the sample used suggest its excellent durability for NRR should be ascribed to the well-maintained nitrogen vacancies in PCN-VN.

Apart from the studies of the chemical mechanisms of metal-free NRR, Rondinone and co-workers employed CMFCs composed of N-doped carbon nanospikes (CNSs) to illustrate the enhancement due to electric fields on NRR.[39] As shown in **Figure 3**G, the CNS surface features a unique morphology of abundant-oriented nanospikes (~ 50 to 80 nm in length), and each nanospike consists of layers of carbon ending in a ~1-nm-wide sharp tip. The sharp tips in the CNS would markedly amplify the local electric field, which may act as “physical catalysts” for ammonia fixation by tuning the molecular orbital energy levels of N_2. As a control, oxygen plasma-etched (O-etched) CNS without the sharp tip texture was also prepared for elucidating the role of sharp tips in NRR. Subsequently, the as-prepared samples were evaluated in neutral electrolytes at ambient

temperature and pressure. **Figure 3**H shows that the rate of ammonia formation at the CNS electrode increases with rising negative potential to -1.19 V, where a maximum ammonia formation rate of ~ 97.18 μg h^{-1} cm^{-2} was achieved. Notably, the production rate of CNS is higher than all the recent reported metal-based NRR electrocatalysts (**Table 1**).[6,40] The FE of the as-prepared CNS at -1.19 V can be as high as ~ 11.56 %, which also superior to most of the recently reported metal-based catalysts (**Table 1**), strongly demonstrating the significance of developing CMFCs to the efficient convertion N_2 into NH_3. However, very little or no ammonia can be detected for O-etched CNS samples at each applied potential. To investigate the electric field effect on NRR, high-level electron propagator theory (EPT) calculations were carried out. The CNS with sharp tips was found to be energetically favorable for NRR by injecting electrons into the antibonding orbitals of N_2 under strong applied electric fields. In comparison, the electric field induced by the O-etched CNS is much weaker and therefore unable to convert N_2 into NH_3, limiting its ammonia production rate. Futhermore, the presence of counter-ions in the aqueous electrolyte was also found to be important, with the observed ammonia production rates decreased in the order of Li^+>Na^+>K^+ (**Figure 3**I). This means that the use of the smallest counterion (Li^+) is beneficial for enhancing the electric field at the sharp spikes and increasing N_2 concentration within the Stern layer. Additionally, the competitive hydrogen evolution reaction is inhibited by the formation of a dehydrated cation layer surrounding the tip, which is conducive to allow access of the N_2 molecule to the high electric field.

4. Conclusion and Outlook

In summary, we have reviewed recent advances in the development of the CMFCs for electrocatalytic NRR under ambient conditions (**Table 2**). Although significant progress has been made by controlling dopant species, engineering surface defects as well as constructing multi-

dimensional carbon architectures, insightful understanding of the catalytic mechanism to further improve the performance of NRR catalysts is still very much needed for practical applications.

NRR pathways are possible from a thermodynamic point of view at room temperature and the CMFCs exhibit promising reaction rates and Faradaic efficiencies for electrocatalytic NRR. In general, electrocatalytic NRR on the surface of a heterogeneous catalyst is believed to involve two broad classes of reaction mechanism: associative and dissociative.[41] In an associative mechanism, the two nitrogen centers bind together as an N_2 molecule is hydrogenated. The product (NH_3) is released along with the cleavage of the N-N bond. Hydrogenation in the associative mechanism can occur through two possible ways, i.e. distal and alternating pathways. Assuming an end-on coordination mode for the N_2, hydrogenation in the distal pathway occurs preferentially on the nitrogen furthest away from the surface of catalyst, leading to the release of an NH_3 molecule and leaving behind a metal nitrido (MN) unit to generate the second NH_3 molecule by reacting with the H^+. The alternative pathway requires each of the two nitrogen centers to be alternated between the two N atoms on the catalytic surface, and the second NH_3 molecule will be released immediately following the removal of the first NH_3 molecule. As distinct from the associative mechanism, the dissociative mechanism involves the cleavage of the N≡N bond before hydrogenation occurs, forming adsorbed N-atoms on the catalytic surface followed by the final step that produces NH_3, eventually regenerating the active site. However, the exact catalytic mechanism and the true active sites are still unclear for carbon-based metal-free NRR. Therefore, an advanced strategy to synergistically combine theoretical studies with some powerful in-situ characterization techniques, such as in-situ X-ray photoelectron spectroscopy, in-situ synchrotron radiation techniques and in-situ defect-characterization, is necessary to gain fundamental understanding of the catalytic mechanism on

surface of CMFCs (e.g. associative or dissociative mechanism; reaction pathways and related intermediate products; electronic structures of CMFCs). It is expected that the suggested research approach will provide novel insights into the NRR mechanism, thereby offering new perspectives on the design of high-performance NRR CMFCs.

Second, the production rates and yields of the CMFCs still need to be improved further by efficient strategies such as heteroatom doping, nano-meso-macro structure design, as well as chemical functionalization of the carbon frameworks. It is well known that NRR requires a high input of energy to split the strong N≡N bond (~ 945.6 kJ mol^{-1}). Such energy is significantly higher than that required to break the C=O bond (750 kJ mol^{-1}) in CO_2RR, indicating that NRR is a much more challenging reaction. Thus, tuning surface states (defects or hydrophilic-hydrophobic property), controlling atom doping, and tailoring atomic and electronic structures are vital to enhance the catalytic activity and suppress the competing hydrogen evolution reaction (HER), thereby benefitting both the efficiency and selectivity of NRR. To the best of our knowledge, there have been no reports to date of P, S or co-doped CMFCs for NRR. Because the dopant (e.g. electronegativity and species) is a key for tuning the electronic configuration and charge redistribution, it could offer an efficient way to develop highly active NRR CMFCs by co-doping or tri-doping. Apart from the high bond energy of the N≡N triple bond, the poor adsorption and low solubility of N_2 molecules in aqueous solution are further obstacles for the yield and production rate of electrochemical NRR. From a kinetic point of view, three-dimensional materials with high porosity have a great advantage for the adsorption and diffusion of N_2 molecules, which is a prerequisite for achieving high yields from NRR. Apart from activity and efficiency, the product-induced pH change of reaction surface can affect the FE and selectivity of NRR, as their reaction pathways depend on the environment around the active centers.

Therefore, fabrication of surface self-adaptive catalysts by molecular doping or functionalization is a promising way to achieve stable and efficient NRR.

Last, the NRR electrolyte selection and products detection are important to ensure genuine positive results are achieved. Liquid electrolytes and solid-state electrolytes are the two main types of electrolytes used during electrocatalytic NRR. Various liquid electrolytes (e.g. aqueous KOH, aqueous HCl, aqueous Li_2SO_4, mixed alcohol/water) have been investigated for electrocatalytic NRR, suggesting that the solubility of N_2 in the electrolytes has a strong correlation with the production rates. Alternatively, electrocatalytic NRR with the solid-state electrolytes, especially Nafion membranes as solid H^+ conductors, are considered to be promising for enhancing the mass transfer of N_2 toward the catalyst surface and inhibiting the occurrence of the HER, thereby effectively overcoming the low conversion and FE of NRR. So, applying gas delivery device structures, such as a gas diffusion electrode (GDE),[27] will be important in the NRR field. On the other hand, as an emerging field, the quantitative detection of the amount of product is crucial to avoid the possibility of false-positive results. Currently, Nessler, phenate and indophenol blue tests are widely used for ammonia or ammonium ion detection. However, certain ions dissolved in solution or contained in the catalysts itself may interfere with these related colorimetric measurements. Particularly for N-doped catalysts, it is strongly recommended that ^{15}N isotope tracer experiments should be performed to determine the source of nitrogen elements in the products. It is also suggested that at least two detection methods (e.g., colorimetric assay, nuclear magnetic resonance and ion chromatography) should be used to determine the amount of product and study the correlation between yield and reaction time.

Supporting Information ((delete if not applicable))

Supporting Information is available from the Wiley Online Library or from the author.

Acknowledgements

((Acknowledgements, general annotations, funding. Other references to the title/authors can also appear here, such as "Author 1 and Author 2 contributed equally to this work."))

Received: ((will be filled in by the editorial staff))

Revised: ((will be filled in by the editorial staff))

Published online: ((will be filled in by the editorial staff))

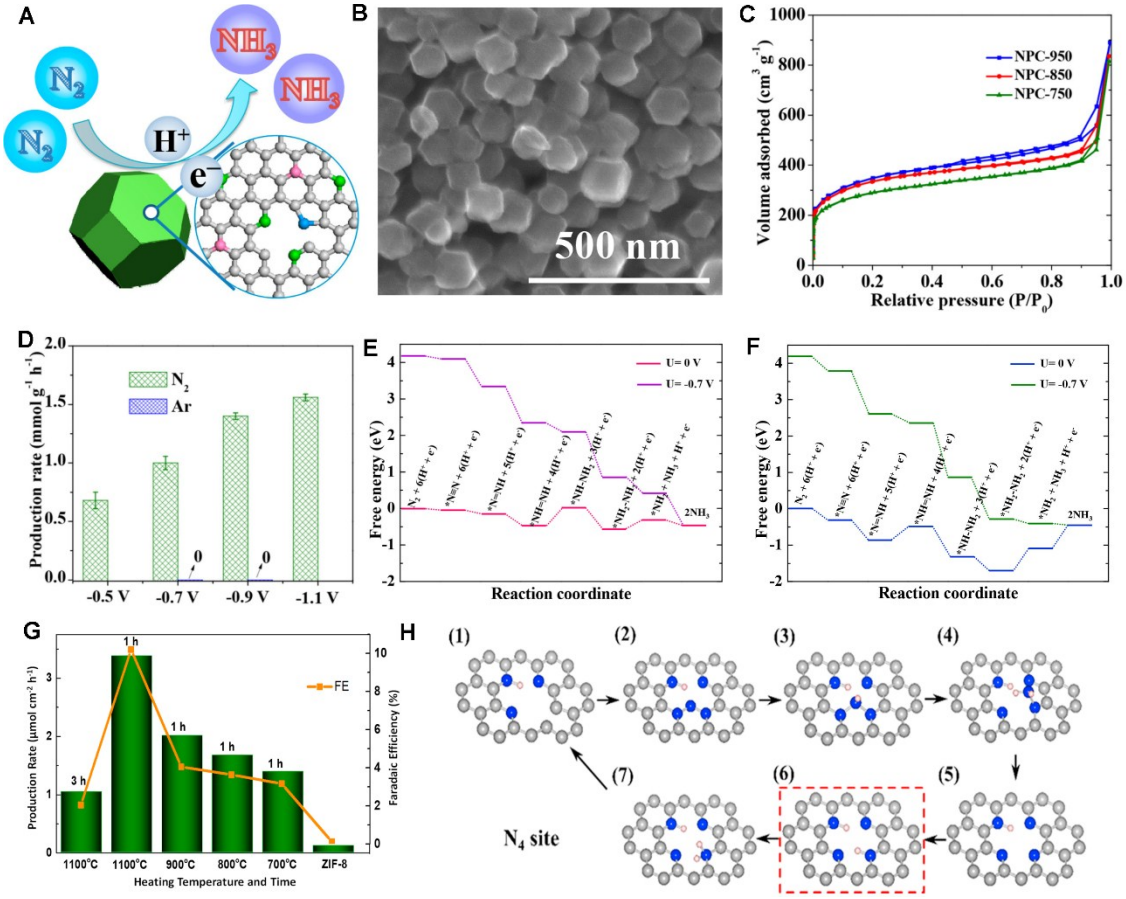

Figure 1. A) Schematic illustration of NPC for NRR. B,C) SEM image and N_2 adsorption-desorption isotherms of NPC. D) Ammonia production rates of NPC-750. E,F) Free energy diagram of NRR on pyridinic and pyrrolic N sites of NPC. Reproduced with permission.[23] Copyright 2018, American Chemical Society. G) Corresponding NH_3 production rates and FEs measured with various catalysts, H) Atomistic structure scheme illustrating the reaction pathway of the NRR on the N_3 sites. The blue, gray, and white balls represent N, C, and H atoms, respectively. Reproduced with permission.[1d] Copyright 2018, Elsevier.

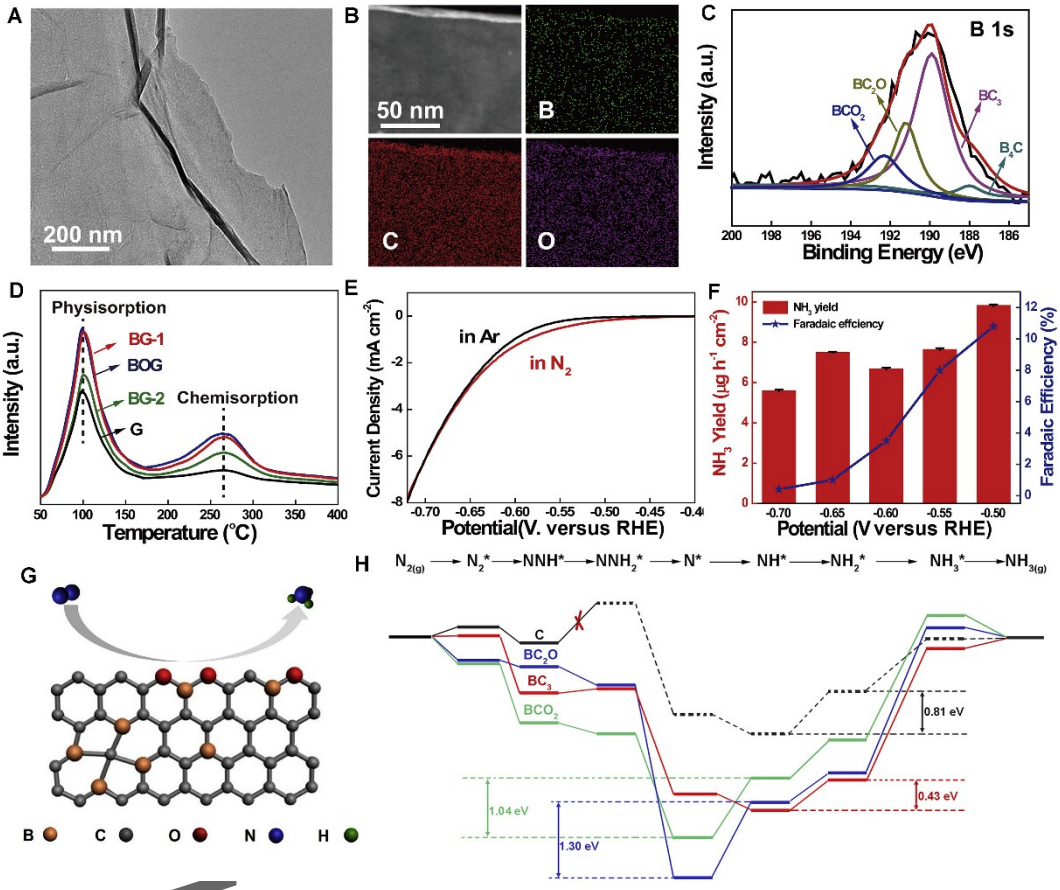

Figure 2. A,B) TEM image and EDS mappings of BG. C) B 1s XPS spectra of BG. D) N_2 TPD curve of the as-prepared samples (mass ratios of H_3BO_3 to graphene oxide were set as 5:1 and 1:10, and the products were defined as BG-1 and BG-2; a mixture of H_3BO_3/graphene oxide (5:1) was annealed in Ar instead of H_2/Ar, designated as BOG). E,F) LSV curves of BG in Ar- and N_2-saturated solutions, and the NH_3 production rates and FE of BG. G) Schematic illustration of NRR for BG. H) Free energy diagrams of NRR on the possible active sites (BC_3, BC_2O, BCO_2, and C). Reproduced with permission.[31] Copyright 2018, Elsevier.

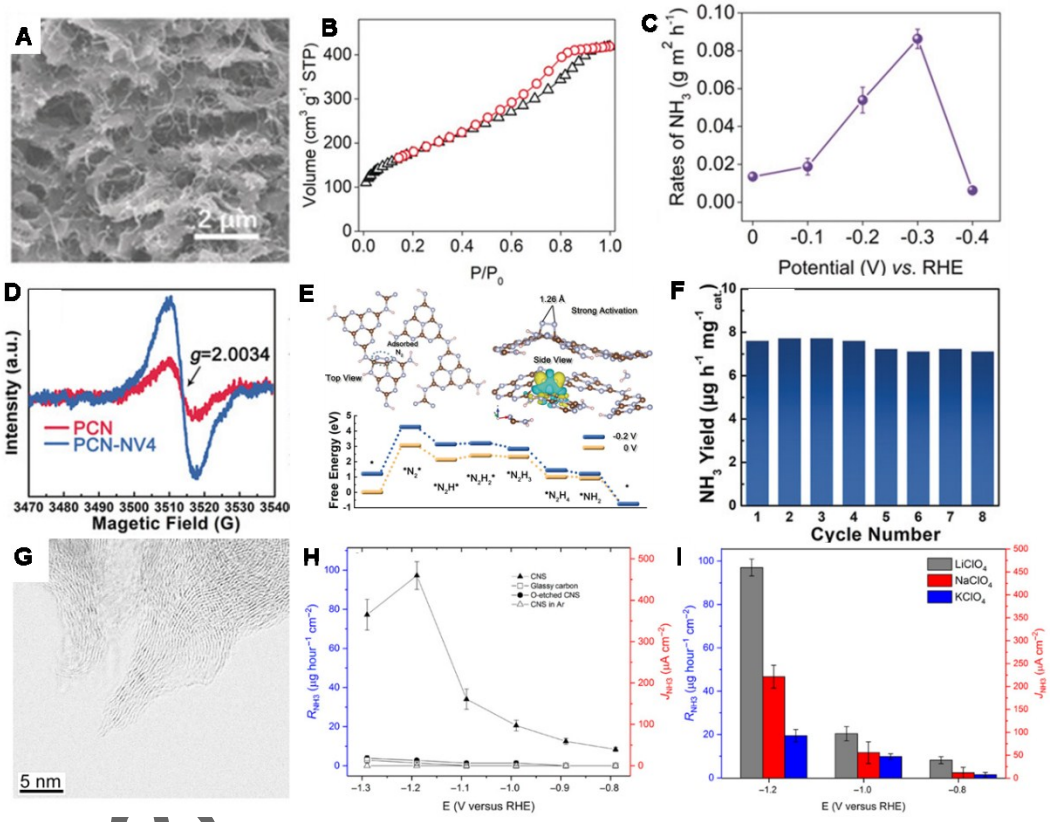

Figure 3. A, B) High-magnification cross-section SEM image and BET specific surface area of NCM. C) The rates of NH_3 production on the NCM electrode. Reproduced with permission.[18] Copyright 2018, Wiley-VCH. D) EPR spectra of PCN-NV, E) The charge density analysis and free energy diagram for NRR on PCN-NV. F) Cycling test of PCN-NV. Reproduced with permission.[19] Copyright 2018, Wiley-VCH. G) Aberration-corrected scanning transmission electron microscopy (STEM) images of CNSs with sharp tips. H) The NH_3 production rates of the as-prepared samples. I) Comparison of electrolyte counterion effects for Li^+ (gray), Na^+ (red), and K^+ (blue). Reproduced with permission.[39] Copyright 2018, AAAS.

Table 1. Comparison of the N_2 electrochemical reduction activity for a metal-free catalyst (CNS) with other metal-based catalysts.

Temp.	Catalysts	Electrolytes	FE (%)	Production rate of NH_3	Refs
25 °C	PEBCD/C	0.5 M Li_2SO_4	2.85	1.68 μg h^{-1} cm^{-2}	[6b]
25 °C	Au nanorod	0.1 M KOH	4.02	1.65 μg h^{-1} cm^{-2}	[26]
20 °C	Au/TiO_2	0.1 M HCl	8.11	21.4 μg h^{-1} mg_{cat}^{-1}	[4b]
25 °C	a-Au/Ce_x-RGO	0.1 M HCl	10.1	8.3 μg h^{-1} mg_{cat}^{-1}	[4a]
25 °C	Fe_2O_3-CNT	0.1 M $KHCO_3$	1.43	0.22 μg h^{-1} cm^{-2}	[27]
25 °C	$Bi_4V_2O_{11}/CeO_2$	0.1 M HCl	10.16	23.21 μg $h^{-1}mg_{cat}^{-1}$	[3]
R.T	VN nanowires	0.1 M HCl	3.58	2.48×10^{-10} mol s^{-1} cm^{-2}	[7c]
R.T	Rh NNs	0.1 M KOH	0.217	23.88 μg h^{-1} mg_{cat}^{-1}	[6d]
20 °C	AuHNCs	0.5 M $LiClO_4$	30.2	3.9 μg h^{-1} cm^{-2}	[40]
80 °C	Pt/C	0.1 M Li_2SO_4	0.83	9.4×10^{-10} mol s^{-1} cm^{-2}	[6c]
90 °C	MOF-Fe	H_2O	1.43	2.1×10^{-10} mol s^{-1} cm^{-2}	[7d]
R.T	Ru SAs/N-C	0.5 M H_2SO_4	29.6	30.84 μg h^{-1} cm^{-2}	[8a]
R.T	N-doped CNS	0.25 M	11.56	97.18 μg h^{-1} cm^{-2}	[39]

	Li_2SO_4		or 5.7 ± 0.4 μmol cm^{-2} h^{-1}		

Table 2. Recent research advances in carbon-based metal-free electrocatalysts for NRR under ambient conditions.

Cat.	Electrolytes	FE (%)	NH_3 production rate	Potential (V vs RHE)	Refs
NPC	0.05 M H_2SO_4	1.43	1.40 mmol cm^{-2} s^{-1}	-0.9 V	[23]
BG-1	0.05 M H_2SO_4	10.8	9.8 μg h^{-1} cm^{-2}	-0.5 V	[31]
NCM	0.1 M HCl	5.2	8 μg h^{-1} cm^{-2}	-0.2 V for FE -0.3 V for production rate	[18]
PCN-NV	0.1 M HCl	11.59	8.09 mg h^{-1} mg_{cat}^{-1}	-0.2 V	[19]
C-ZIF-1100	0.1 M KOH	10.2	3.4 μmol cm^{-2} h^{-1}	-0.3 V	[1d]
CNS	0.25 M Li_2SO_4	11.56	97.18 μg h^{-1} cm^{-2}	-1.19 V	[39]

References

[1] a) B. M. Hoffman, D. Lukoyanov, Z.-Y. Yang, D. R. Dean, L. C. Seefeldt, *Chem. Rev.* **2014**, *114*, 4041; b) M.-A. Légaré, G. Bélanger-Chabot, R. D. Dewhurst, E. Welz, I. Krummenacher, B. Engels, H. Braunschweig, *Science* **2018**, *359*, 896; c) Y. Gong, J. Wu, M. Kitano, J. Wang, T.-N. Ye, J. Li, Y. Kobayashi, K. Kishida, H. Abe, Y. Niwa, H. Yang, T. Tada, H. Hosono, *Nature Catalysis* **2018**, *1*, 178; d) S. Mukherjee, D. A. Cullen, S. Karakalos, K. Liu, H. Zhang, S. Zhao, H. Xu, K. L. More, G. Wang, G. Wu, *Nano Energy* **2018**, *48*, 217.

[2] U. S. G. Survey, O. S, U. S. G. Survey, *Mineral Commodity Summaries, 2009*, U.S. Government Printing Office, **2009**.

[3] C. Lv, C. Yan, G. Chen, Y. Ding, J. Sun, Y. Zhou, G. Yu, *Angew. Chem.* **2018**, *130*, 6181.

[4] a) S-J. Li, D. Bao, M-M. Shi, B-R. Wulan, J-M. Yan, Q. Jiang, *Adv. Mater.* **2017**, *29*, 1700001; b) M-M. Shi, D. Bao, W. B-R. Wulan, Y-H. Li, Y-F. Zhang, J-M. Yan, Q. Jiang, *Adv. Mater.* **2017**, *29*, 1606550. c) S. L. Foster, S. I. Perez Bakovic, R. D. Duda, S. Maheshwari, R. D. Milton, S. D. Minteer, M. J. Janik, J. N. Renner, L. F. Greenlee, *Nature Catalysis* **2018**, *1*, 490.

[5] H. Davy, *Philosophical Transactions of the Royal Society of London* **1807**, *97*, 1.

[6] a) N. Cao, G. Zheng, *Nano Research* **2018**, *11*, 2992; b) G-G, Chen, X. Cao, S. Wu, X. Zeng, L-X. Ding, M. Zhu, H. Wang, *J. Am. Chem. Soc.* **2017**, *139*, 9771; c) R. Lan, S. Tao, *RSC Adv.* **2013**, *3*, 18016;

d) H-M. Liu, S-H. Han, Y. Zhao, Y-Y. Zhu, X-L. Tian, J-H. Zeng, J-X. Jiang, B. Xia, Y. Chen, *J. Mater. Chem. A* **2018**, *6*, 3211.

[7] a) H.-P. Jia, E. A. Quadrelli, *Chem. Soc. Rev.* **2014**, *43*, 547; b) Y. Yao, S. Zhu, H. Wang, H. Li, M. Shao, *J. Am. Chem. Soc.* **2018**, *140*, 1496; c) X. Zhang, R-M. Kong, H. Du, L. Xia, F. Qu*, Chem. Commun.* **2018**, 54, 5323; d) X. Zhao, F. Yin, N. Liu, G. Li, T. Fan, B. Chen, *J. Mater. Sci.* **2017**, 52, 10175.

[8] a) Z. Geng, Y. Liu, X. Kong, P. Li, K. Li, Z. Liu, J. Du, M. Shu, R. Si, J. Zeng, *Adv. Mater.* **2018**, *30*, 1803498; b) C. Guo, J. Ran, A. Vasileff, S.-Z. Qiao, *Energy Environ. Sci.* **2018**, *11*, 45.

[9] a) E. Skúlason, T. Bligaard, S. Gudmundsdóttir, F. Studt, J. Rossmeisl, F. Abild-Pedersen, T. Vegge, H. Jónsson, J. K. Nørskov, *Phys. Chem. Chem. Phys.* **2012**, *14*, 1235; b) Z. Yao, J. Yan, J. Mietek, Q. S. Zhang, *Angew. Chem. Int. Ed.* **2015**, *54*, 52.

[10] G.-F. Chen, X. Cao, S. Wu, X. Zeng, L.-X. Ding, M. Zhu, H. Wang, *J. Am. Chem. Soc.* **2017**, *139*, 9771.

[11] a) F. Rodríguez-reinoso, *Carbon*, **1998**, *36*, 159; b) K. Gong, F. Du, Z. Xia, M. Durstock, L. Dai, *Science* **2009**, *323*, 760.

[12] a) X. Liu, L. Dai, *Nat. Rev. Mater.* **2016**, *1*, 16064; b) X. Lu, W.-L. Yim, B. H. R. Suryanto, C. Zhao, *J. Am. Chem. Soc.* **2015**, *137*, 2901; c) Z. Xu, X. Zhuang, C. Yang, J. Cao, Z. Yao,Y. Tang, J. Jiang, D. Wu, X. Feng, *Adv. Mater.* **2016**, *28*, 1981.

[13] a) Y. Jiao, Y. Zheng, K. Davey, S.-Z. Qiao, *Nat. Energy* **2016**, *1*, 16130; b) J-X. Feng, H. Xu, S-H. Ye, G. Ouyang, Y-X. Tong, G-R. Li, *Angew. Chem. Int. Ed.* **2017**, *56*, 8120.

[14] a) X. Lu, T-H. Tan, Y. Ng, R. Amal, *Chemistry - A European Journal* **2016**, *22*, 11991; b) Y. Song, W. Chen, C. Zhao, S. Li, W. Wei, Y. Sun, *Angew. Chem.* **2017**, *129*, 10980; c) J. Xie, X. Zhao, M. Wu, Q. Li, Y. Wu, J. Yao, *Angew. Chem. Int. Ed.* **2018**, *57*, 9640.

[15] a) J. Zhang, Z. Zhao, Z. Xia, L. Dai, *Nat. Nanotechnol.* **2015**, *10*, 444; b) C. Hu, L. Dai, *Adv. Mater.* **2017**, *29*, 1604942; c) Y. Jia, L. Zhang, A. Du, G. Gao, J. Chen, X. Yan, C. L. Brown, X. Yao, *Adv. Mater.* **2016**, *28*, 9532.

[16] H.-W. Liang, Z.-Y. Wu, L.-F. Chen, C. Li, S.-H. Yu, *Nano Energy* **2015**, *11*, 366.

[17] a) L. Dai, *Acc. Chem. Res.* **2013**, *46*, 31; b) T. Zhang, Y. Hou, V. Dzhagan, Z. Liao, G. Chai, M. Löffler, D. Olianas, A. Milani, S. Xu, M. Tommasini, D. R. T. Zahn, Z. Zheng, E. Zschech, R. Jordan, X. Feng, *Nat. Commun.* **2018**, *9*, 1140; c) J. Zhang, G. Chen, K. Müllen, X. Feng, *Adv. Mater.*, *0*, 1800528; d) H. Tian, N. Wang, F. Xu, P. Zhang, D. Hou, Y. Mai, X. Feng, *J. Mater. Chem. A* **2018**, *6*, 10354.

[18] H. Wang, L. Wang, Q. Wang, S. Ye, W. Sun, Y. Shao, Z. Jiang, Q. Qiao, Y. Zhu, P. Song, D. Li, L. He, X. Zhang, J. Yuan, T. Wu, G. A. Ozin, *Angew. Chem. Int. Ed.*, **2018**, DOI: 10.1002/anie.201805514.

[19] C. Lv, Y. Qian, C. Yan, Y. Ding, Y. Liu, G. Chen, G. Yu, *Angew. Chem. Int. Ed.* **2018**, *57*, 10246.

[20] a) Y. Zheng, Y. Jiao, Y. Zhu, Q. Cai, A. Vasileff, L. H. Li, Y. Han, Y. Chen, S.-Z. Qiao, *J. Am. Chem. Soc.* **2017**, *139*, 3336; b) D. Li, Y. Jia, G. Chang, J. Chen, H. Liu, J. Wang, Y. Hu, Y. Xia, D. Yang, X. Yao, *Chem* **2018**, doi.org/10.1016/j.chempr.2018.07.005.

[21] C. Hu, L. Dai, *Adv. Mater.* **2017**, *29*, 1604942.

[22] Z. Xu, X. Zhuang, C. Yang, J. Cao, Z. Yao, Y. Tang, J. Jiang, D. Wu, X. Feng, *Adv. Mater.* **2016**, *28*, 1981.

[23] Y. Liu, Y. Su, X. Quan, X. Fan, S. Chen, H. Yu, H. Zhao, Y. Zhang, J. Zhao, *ACS Catal.* **2018**, *8*, 1186.

[24] D. S. Su, S. Perathoner, G. Centi, *Chem. Rev.* **2013**, *113*, 5782.

[25] V. Kordali, G. Kyriacou, C. Lambrou, *Chem. Commun.* **2000**, 1673.

[26] D. Bao, Q. Zhang, F.-L. Meng, H.-X. Zhong, M.-M. Shi, Y. Zhang, J.-M. Yan, Q. Jiang, X.-B. Zhang, *Adv. Mater.* **2017**, *29*, 1604799.

[27] S. Chen, S. Perathoner, C. Ampelli, C. Mebrahtu, D. Su, G. Centi, *Angew. Chem. Int. Ed.* **2017**, *56*, 2699.

[28] R. Lan, J. T. S. Irvine, S. Tao, *Sci. Rep.* **2013**, *3*, 1145.

[29] L. Yang, S. Jiang, Y. Zhao, L. Zhu, S. Chen, X. Wang, Q. Wu, J. Ma, Y. Ma, Z. Hu, *Angew. Chem. Int. Ed.* **2011**, *50*, 7132.

[30] a) N. Sreekanth, M. A. Nazrulla, T. V. Vineesh, K. Sailaja, K. L. Phani, *Chem. Commun.* **2015**, *51*, 16061; b) C. Hering-Junghans, *Angew. Chem. Int. Ed.* **2018**, *57*, 6738.

[31] X. Yu, P. Han, Z. Wei, L. Huang, Z. Gu, S. Peng, J. Ma, G. Zheng, *Joule* **2018**, doi.org/10.1016/j.joule.2018.06.007.

[32] C. Wang, Z. Guo, W. Shen, Q. Xu, H. Liu, Y. Wang, *Adv. Funct. Mater.* **2014**, *24*, 5511.

[33] C. V. S. Kumar, V. Subramanian, *Phys. Chem. Chem. Phys.* **2017**, *19*, 15377.

[34] a) C. Tang, Q. Zhang, *Adv. Mater.* **2017**, *29*, 1604103; b) S. Zhao, Y. Wang, J. Dong, C.-T. He, H. Yin, P. An, K. Zhao, X. Zhang, C. Gao, L. Zhang, J. Lv, J. Wang, J. Zhang, A. M. Khattak, N. A. Khan, Z. Wei, J. Zhang, S. Liu, H. Zhao, Z. Tang, *Nat. Energy* **2016**, *1*, 16184; c) S. Zhao, Y. Li, H. Yin, Z. Liu, E. Luan, F. Zhao, Z. Tang, S. Liu, *Sci. Adv.* **2015**, *1*.

[35] a) Y. Meng, D. Voiry, A. Goswami, X. Zou, X. Huang, M. Chhowalla, Z. Liu, T. Asefa, *J. Am. Chem. Soc.* **2014**, *136*, 13554; b) S. Zhao, H. Yin, L. Du, L. He, K. Zhao, L. Chang, G. Yin, H. Zhao, S. Liu, Z. Tang, *ACS Nano* **2014**, *8*, 12660.

[36] a) S. Wan, J. Qi, W. Zhang, W. Wang, S. Zhang, K. Liu, H. Zheng, J. Sun, S. Wang, R. Cao, *Adv. Mater.* **2017**, *29*, 1700286; b) X. Duan, J. Xu, Z. Wei, J. Ma, S. Guo, S. Wang, H. Liu, S. Dou, *Adv. Mater.* **2017**, *29*, 1701784; c) S. Zhao, H. Yin, L. Du, G. Yin, Z. Tang, S. Liu, *J. Mater. Chem. A* **2014**, *2*, 3719; d) L. Dai, Y. Xue, L. Qu, H.-J. Choi, J.-B. Baek, *Chem. Rev.* **2015**, *115*, 4823.

[37] a) Z. Hong, B. Shen, Y. Chen, B. Lin, B. Gao, *J. Mater. Chem. A* **2013**, *1*, 11754; b) M. K. Bhunia, K. Yamauchi, K. Takanabe, *Angew. Chem.* **2014**, *126*, 11181.

[38] M. P. Shaver, M. D. Fryzuk, *Adv. Synth. Catal.* **2003**, *345*, 1061.

[39] Y. Song, D. Johnson, R. Peng, D. K. Hensley, P. V. Bonnesen, L. Liang, J. Huang, F. Yang, F. Zhang, R. Qiao, A. P. Baddorf, T. J. Tschaplinski, N. L. Engle, M. C. Hatzell, Z. Wu, D. A. Cullen, H. M. Meyer, B. G. Sumpter, A. J. Rondinone, *Sci. Adv.* **2018**, *4*, e1700336.

[40] M. Nazemi, S. R. Panikkanvalappil, M. A. EI-Sayed, *Nano Energy* **2018**, *49*, 316.

[41] M. A. Shipman, M. D.Symes, *Catalysis Today*, **2017**, *286*, 57.

Emerging carbon-based metal-free catalysts have been demonstrated to be promising alternatives to noble metal/metal oxide catalysts for electrocatalytic NRR at ambient conditions. Recent advances in the development of carbon-based metal-free catalysts for electrocatalytic nitrogen fixation are discussed, and the key challenges and future opportunities in this exciting field are highlighted.

Metal-Free Catalysts